

Galactic archaeology of a thick disc: Excavating ESO 533-4 with VIMOS [★]

S. Comerón^{1,2}, H. Salo¹, J. Janz³, E. Laurikainen¹, and P. Yoachim⁴

¹ University of Oulu, Astronomy and Space Physics, P.O. Box 3000, FI-90014, Finland
e-mail: seb.comeron@gmail.com

² Finnish Centre of Astronomy with ESO (FINCA), University of Turku, Väisäläntie 20, FI-21500, Piikkiö, Finland

³ Centre for Astrophysics and Supercomputing, Swinburne University, Hawthorn, VIC 3122, Australia

⁴ Department of Astronomy, University of Washington, Box 351580, Seattle, WA 98195, USA

Preprint online version: October 12, 2018

ABSTRACT

The disc of galaxies is made of the superposition of a thin and a thick disc. Star formation is hosted in the thin discs and contributes to their growth. Thick discs are formed of old stars. The formation mechanisms of thick discs are under discussion. Thick discs might have formed either at high redshift on a short timescale or might have been built slowly over a Hubble-Lemaître time. They may have an internal or an external origin. Here we adopt a galactic archaeology approach to study the thick disc of ESO 533-4, i.e. we study the kinematics and the stellar populations of this galaxy in detail. ESO 533-4 is a Southern, nearby, and almost bulgeless galaxy. We present the first ever Integral Field Unit spectroscopy of an edge-on galaxy with enough depth and quality to study the thick disc. We exposed ESO 533-4 with the blue grism of the VIMOS instrument of the VLT for 6.5 hours. The field of view covered an axial extent from $\sim 0.1 r_{25}$ to $\sim 0.7 r_{25}$, where r_{25} is the 25 mag arcsec⁻² isophotal radius. This corresponds to the range from ~ 1 kpc to ~ 7 kpc. We used pPXF and the MILES library to obtain velocity and stellar population maps. We compared our kinematic data with simple GADGET-2 models.

The apparent rotational lag of the thick disc of ESO 533-4 is compatible with that expected from the combinations of two effects: differential asymmetric drift and the projection effects arising from studying a disc a few degrees ($2 - 3^\circ$) away from edge-on. Thus, ESO 533-4 contains little or no counter-rotating material. This is compatible with three formation scenarios: the secular dynamical heating of an initially thin disc, the formation of the thick disc at high redshift in an early turbulent disc phase, and the creation of a thick disc in a major merger event. If this last mechanism occurred in all galaxies, it would cause retrograde thick discs in half of them. These retrograde discs have not been observed in the five massive disc galaxies (circular velocity $v_c \gtrsim 120$ km s⁻¹) for which the kinematics of the thick disc is known. The stellar populations map indicates that the populations of the thin and the thick discs of ESO 533-4 are possibly separated in the Age – $\log(Z/Z_\odot)$ plane. This would imply that thin and thick discs are formed of two distinct stellar populations. The stellar population results are not fully conclusive because of the high dust extinction in ESO 533-4 and because recovering stellar populations is a difficult inverse problem. Having said that, the stellar population results do not favour a secular evolution origin for the thick disc. Hence, we suggest that the thick disc of ESO 533-4 formed in a relatively short event.

Key words. galaxies: individual (ESO 533-4) – galaxies: kinematics and dynamics – galaxies: spiral – galaxies: structure – galaxies: evolution – galaxies: formation

1. Introduction: Thick discs and galactic archaeology

We know with absolute certainty that our universe contains galaxies (Curtis 1917; Öpik 1922; Hubble 1925). Another fact established with almost the same degree of certitude is that the initial state of the universe was a hot Big Bang (Lemaître 1931; Gamow 1946; Alpher & Herman 1949; Penzias & Wilson 1965). It follows that the products of the primordial nucleosynthesis somehow assembled and evolved into the galaxies that we observe roughly a Hubble-Lemaître time after creation. The current cosmological paradigm is Lambda cold dark matter (Λ CDM; Planck Collaboration 2015, for a recent parameter determination), where the energy budget of the universe is dominated by elusive dark matter and a positive cosmological constant. Within that paradigm, the evolution of galaxies is driven by a combination of interactions with the environment

(nurture; e.g. Toomre 1977) and internal evolution (nature; e.g. Kormendy & Kennicutt 2004; Athanassoula 2013). However, the details and the specific weight of each of these two families of processes in the galaxy construction and subsequent evolution still elude us.

One of the most mysterious remnants of galaxy formation and evolution are thick discs. Seen as roughly exponential vertical excesses of light in edge-on galaxies a few thin disc scale heights above the galaxy mid-planes, their origin is still a matter of debate more than three decennia after their discovery (Burstein 1979; Tsikoudi 1979). Nowadays, all disc galaxies where thick discs have been searched for have been found to host one or even two of them (Yoachim & Dalcanton 2006; Comerón et al. 2011c,b, but see Streich et al. (2015)). The following scenarios have been proposed to explain their formation:

- **External fast processes:** the thick disc is the consequence of the merger of two or more gas-rich galaxies during the initial assembly process (Brook et al. 2004).

[★] Based on observations made at the European Southern Observatory using the Very Large Telescope under programme 091.B-0228(A).

Table 1. Summary of the signatures predicted in the thick disc formation scenarios

Scenario	External/ Internal	Fast/ Secular	Counter-rotating material in the thick disc	Chemical and/or age discontinuity between the thin and thick discs
Merger of gas-rich galaxies	External	Fast	Possibly ^a	Yes
Turbulent early disc	Internal	Fast	No ^b	Yes
Accretion of stars from satellites	External	Secular	Possibly ^a	Yes
Heating by satellites	External	Secular	No	No
Internal heating	Internal	Secular	No	No

^(a) Those processes would cause some amount of counter-rotating material provided that some of the mergers are retrograde. ^(b) In the Bournaud et al. (2014) simulations, some counter-rotating stars are created in this process. The fraction of retrograde stars decreases as a function of the mass of the galaxy. A high- z galaxy with a $1.4 \times 10^{10} M_{\odot}$ baryonic mass, similar to the mass of ESO 533-4's thick disc, would have 2.2% of counter-rotating stars (F. Bournaud, private communication). This small fraction of counter-rotating stars would be undetectable with the techniques used in this paper.

- **Internal fast processes:** the thick disc is born thick because of the turbulent and clumpy nature of the first discs (Elmegreen & Elmegreen 2006; Bournaud et al. 2009; Comerón et al. 2014).
- **External secular processes:** the thick disc is made of stars stripped from infalling satellites (Abadi et al. 2003) and/or by the disc dynamical heating caused by these satellites (Quinn et al. 1993; Qu et al. 2011). We call these processes secular because minor mergers are much slower than major mergers as a result of weaker dynamical friction. Also, according to Λ CDM, several of these events can occur in a Hubble-Lemaître time (e.g. several tens of minor mergers causing tidal features are expected in Johnston et al. 2008).
- **Internal secular processes:** the thick disc is caused by dynamical heating due to disc overdensities (Villumsen 1985) and/or the radial migration of stars (Schönrich & Binney 2009a,b; Loebman et al. 2011). Radial migration as a viable mechanism to build thick discs is contested by Minchev et al. (2012) and Vera-Ciro et al. (2014).

It is likely that a combination of two or more of these scenarios contributed to the thick disc formation. Actually, some mechanisms, such as secular internal heating, must always occur to some extent. In Comerón et al. (2012), we suggested that thick discs in low- and high-mass galaxies might have different dominant formation mechanisms. This is because there is a clear bimodality in the ratio of thick to thin disc masses as a function of the total galaxy mass: high-mass galaxies have the same ratio irrespective of the galaxy total mass, whereas for low-mass galaxies the ratio decreases as the total galaxy mass increases. The fact that most high-mass galaxies have roughly similar thick to thin disc mass ratios (Comerón et al. 2014) suggests the possibility that the same combination of mechanisms built them. The dividing line between low- and high-mass galaxies is found at a circular velocity $v_c \approx 120 \text{ km s}^{-1}$ (suggested by Yoachim & Dalcanton 2006, 2008b), which corresponds to a baryonic mass of $M \sim 10^{10} M_{\odot}$ when using the Tully-Fisher relation in Zaritsky et al. (2014).

A particular model (Schönrich & Binney 2009a,b; Roškar et al. 2013; Minchev et al. 2015), which proposes a thick disc created through a combination of internal and external secular heating mechanisms, is relevant in later sections of the paper. In this model, each of the mono-age populations of a galaxy is distributed in a flared disc. The younger stellar populations have a longer scale length than the older stellar populations. The superposition of a series of flares at different radii produce what has been identified in photometric decompositions as a thick disc. The result of this model is a galaxy with

no apparent flare even if the individual mono-age populations do flare.

As a result of cosmological dimming and resolution problems, it is often impractical to tackle galaxy evolution issues by observing highly redshifted objects. An alternative is so-called galactic archaeology, which consists of studying the structures of redshift $z \sim 0$ galaxies in great detail to infer their origin. Thick discs are ideal targets for galactic archaeology because different formation scenarios predict distinct kinematical and chemical signatures, as summarized in Table 1.

So far, attempts to do galactic archaeology in external edge-on galaxies to study thick discs have been mostly based on photometric decompositions (Yoachim & Dalcanton 2006; Comerón et al. 2011a, 2012). The exception is the work by Yoachim & Dalcanton (2008b,a), in which single-slit spectroscopy was used to study thin and thick discs. They found that thick discs are made of old stars and that thick discs of some low-mass galaxies contain counter-rotating stars. None of the three massive galaxies in their sample had measurable amounts of retrograde stars. The problem that arises from single-slit observations is that one has to rely on photometric decompositions to find the range of heights where the thick disc dominates before placing the slit. Ideally, we would like to be able to observe galaxies in a wide range of heights, so no assumptions about the extent of the thick disc have to be made a priori.

2. ESO 533-4

We present the first integral field spectroscopy study of the thin/thick structure of an edge-on disc. We used the Visible Multi-Object Spectrograph of the Very Large Telescope (VIMOS; Le Fèvre et al. 2003). The selected target was ESO 533-4. This galaxy has been part of the sample of our recent thick disc studies (Comerón et al. 2012, 2014). The target was chosen because of:

- its small central mass concentration (CMC), and hence, presumably little effect of a central spheroid on the thin and thick disc kinematics;
- its relatively small angular size, so a large fraction of the disc could be covered by the VIMOS field of view (FOV); and
- a brighter than average thick disc, which starts to dominate at $m_{3,6\mu\text{m}}(\text{AB}) \approx 22 \text{ mag arcsec}^{-2}$ (Comerón et al. 2012) so that thick disc spectra can be obtained with a few hours of exposure.

A summary of the properties of ESO 533-4 is presented in Table 2. There is a disagreement about the stage of the galaxy in the literature. ESO 533-4 has a small CMC, which makes it

Table 2. Parameters of ESO 533-4

Parameter	Value	Source
RA (J2000.0)	22 ^h 14 ^m 03.02	1
Dec (J2000.0)	-26°56'15".8	1
$M_{3.6\mu\text{m}}(\text{AB})$	-20.52	2
Type	Sc? sp	3
	S0 _c ⁰ sp/E(d)8	4
v_{sys} (helio-centric)	2596 ± 3 km s ⁻¹	5
D	39.8 Mpc	6
1" physical size	193 pc	6
v_c	147.5 ± 2.2 km s ⁻¹	7
r_{25}	54'.6	7
Luminosity profile	Type 2 break	8
M_g	(680 ± 20) × 10 ⁷ M _⊙	9
M_{CMC}	(19 ± 2) × 10 ⁷ M _⊙	9
M_t	(1500 ± 300) × 10 ⁷ M _⊙	10
M_T	(1100 ± 200) × 10 ⁷ M _⊙	10

References. (1) Skrutskie et al. (2006); (2) Muñoz-Mateos et al. (2015); (3) de Vaucouleurs et al. (1991); (4) Buta et al. (2015); (5) NED; (6) from NED average of redshift-independent distances; (7) HyperLeda (Makarov et al. 2014); (8) Comerón et al. (2012); (9) atomic gas disc mass (M_g) and CMC mass (M_{CMC}) from Comerón et al. (2014); (10) thin disc mass (M_t) and thick disc mass (M_T) from this paper.

appear late type (Sc; de Vaucouleurs et al. 1991), but its smooth appearance at 3.6 μm has recently caused it to be classified as an S0_c⁰ (Buta et al. 2015). ESO 533-4 has a baryonic mass $\mathcal{M} \sim 3 \times 10^{10} M_{\odot}$, and hence it is a high-mass galaxy. A 3.6 μm image from the Spitzer Survey of Stellar Structure in Galaxies (S⁴G; Sheth et al. 2010) is presented in Fig. 1.

3. The thin/thick disc decomposition of ESO 533-4

In Comerón et al. (2012), we made thin/thick disc decompositions of ESO 533-4 for the symmetrized 3.6 μm + 4.5 μm luminosity profiles in four bins perpendicular to the galaxy mid-plane. The discs were assumed to be in hydrostatic equilibrium following the formalism by Narayan & Jog (2002). We accounted for the gravitational effect of a thin gas disc with 20% of the surface mass density of the thin disc. We made several simplifying assumptions, such as similar scale lengths for the thin and thick discs, that the disc is not too submaximal in its inner parts, vertical isothermality, and roughly constant scale heights with changing radii.

In Comerón et al. (2012) we convolved our solutions with a Gaussian kernel to account for the point spread function (PSF) of the S⁴G images. The kernel had a 2".2 full width at half maximum (FWHM). However, the S⁴G PSF is now known to have faint but extended wings not accounted for by a Gaussian. Here we redo the fits using the S⁴G symmetrized PSF (Salo et al. 2015). Here we produce our fit using only the 3.6 μm band because we only have a detailed PSF model for that band.

We use the sky values from the S⁴G Pipeline 3 (Muñoz-Mateos et al. 2015) instead of our own sky determinations. To do the fit, we use IDL's CURVEFIT instead of our own minimization routine (described in Comerón et al. 2011a). As in Comerón et al. (2012), we use a ratio of mass-to-light ratios of the thick and thin discs $\Upsilon_T/\Upsilon_t = 1.2$. The $\Upsilon_T/\Upsilon_t = 1.2$ value comes from studying the spectral energy distributions resulting from the Milky Way star formation history models by Nykytyuk & Mishenina (2006) for the thin and the thick discs (Comerón et al. 2011a). The maximum height of the fit

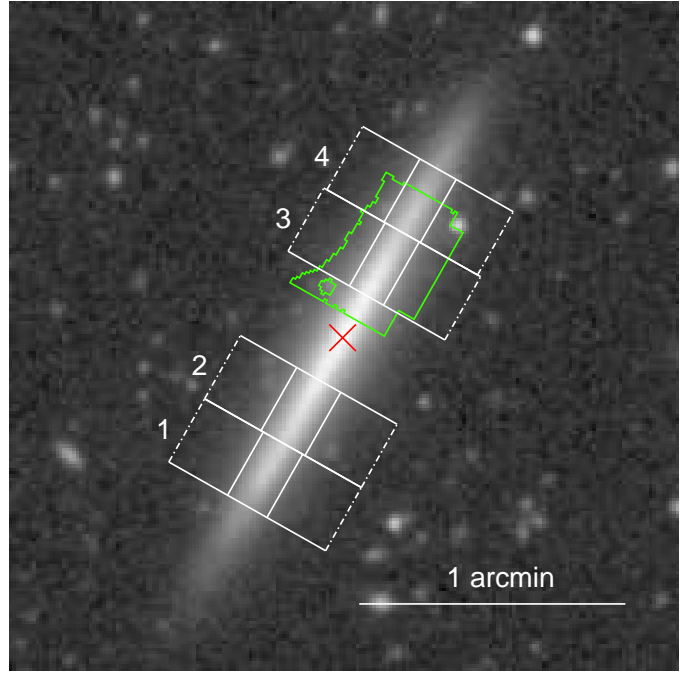


Fig. 1. 3.6 μm image of ESO 533-4 from the S⁴G. The red cross indicates the centre of the galaxy and the region with a green border is that we studied. North is up and east is left. The white solid lines perpendicular to the galaxy mid-plane show the four axial bins used for the luminosity profile fits in Fig. 2. The dash-dotted lines indicate the heights over which the profiles were fit. The solid lines parallel to the galaxy mid-plane correspond to the height above which 90% of the light comes from the thick disc. The numbers are used to associate the bins with the fits in Fig. 2.

was selected as that beyond which it is not possible to make a two disc component fit (the mean squared difference between the observed profile and the fit becomes larger than 0.01 (mag arcsec⁻²)² at that height). What limits the height of the fitting region is the presence of scattered light of point sources in the field and background gradient issues. The extent of the fitting range covers over four thick disc scale heights.

The new thin/thick disc fits are very similar to those in Comerón et al. (2012), which indicates that the errors introduced by approximating the PSF with a Gaussian function were small. The symmetrized PSF used here covers 15" in radius. The thick disc dominates the luminosity profiles down to $z \approx 5''$ (~ 1 kpc), which is a height safely smaller than the radius of the modelled PSF. If we consider our fitted thin disc, we find that the extra light added to $|z| > 5''$ is about 4% of the observed emission. Therefore, we can discard the possibility that the thick disc is an artefact caused by scattered light as suggested by Sandin (2015).

The new fits indicate a slightly higher ratio of surface densities between the thick and thin disc (Σ_T/Σ_t) compared to Comerón et al. (2012), which slightly increases the mass ratio of the two discs: $M_T/M_t = 0.65$ in Comerón et al. (2012) and $M_T/M_t = 0.77$ here, following Eq. 5 in Comerón et al. (2011a). We could use a gas disc surface density larger than 20% of that of the thin disc to reflect the fact that the gas mass is $\sim 45\%$ that of the thin disc (Table 2). However, this would not take into account that usually gas discs are more extended than stellar discs. Furthermore, when we refitted the luminosity profiles with dou-

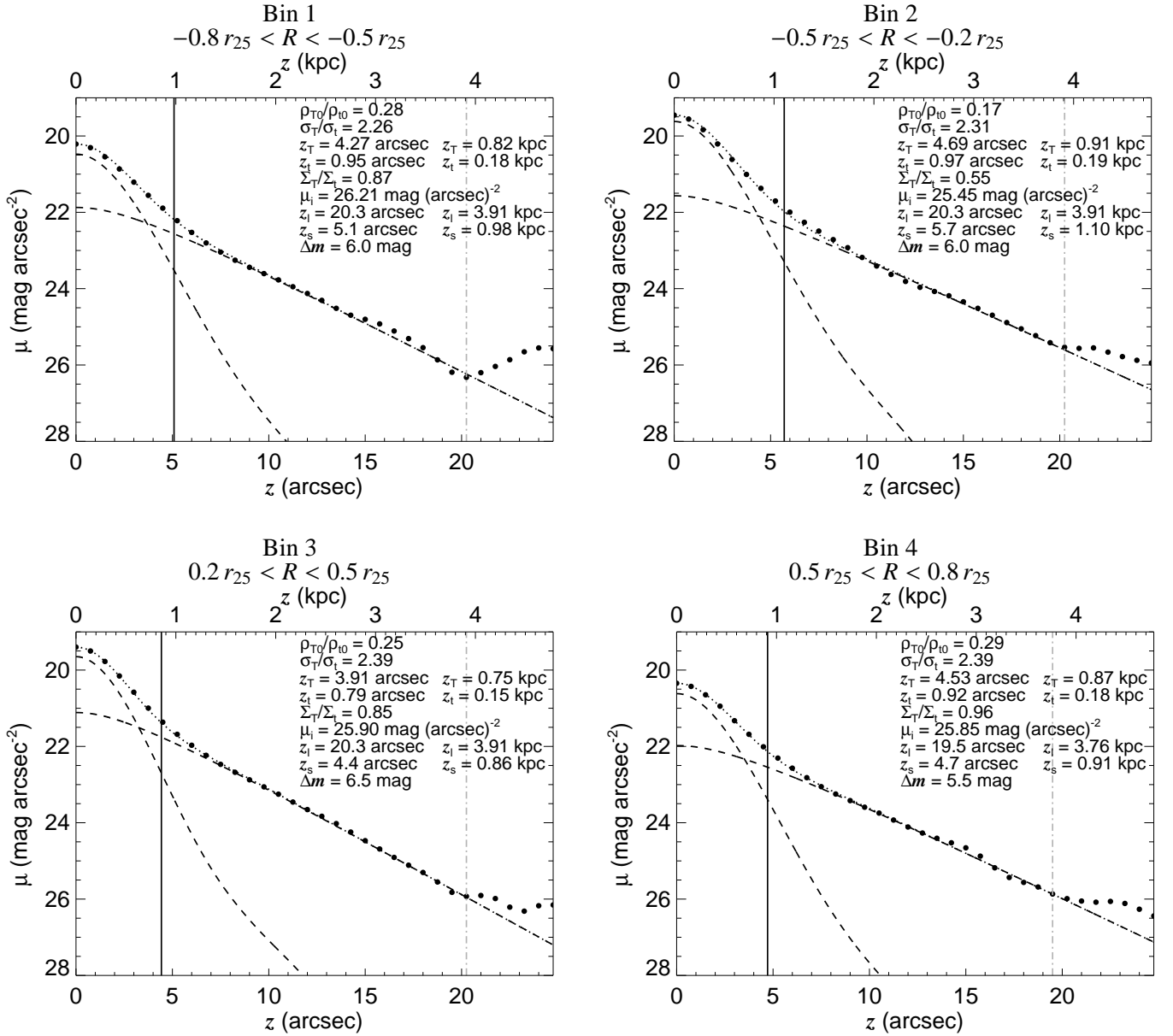


Fig. 2. Luminosity profiles of ESO 533-4 in the four bins perpendicular to the mid-plane that are indicated in Fig. 1 (large dots). The fits are indicated with the dotted lines, and the contribution of the thin and thick discs are indicated with dashed lines. The vertical solid line indicates the height, z_s , above which 90% of the light comes from the thick disc according to our fit. The dot-dashed grey vertical line indicates the maximum height, z_t , that we use for the fit. ρ_{T0}/ρ_{10} stands for the thick to thin disc mass density ratio at the mid-plane, σ_T/σ_t for their velocity dispersion ratio, z_T and z_t for the thick and thin disc vertical scale heights, Σ_T/Σ_t for the thick to thin disc mass ratio, μ_i for the lowest fitted surface brightness level, and Δm for the range in magnitudes over which the fit was done.

ble the gas surface density, we obtained the same M_T/M_t within 1%.

We find that 90% of the light coming from the region $|z| \gtrsim 5''$ ($z \gtrsim 970$ pc) is emitted by the thick disc. In what follows, we consider that region as that where the thick disc dominates the surface brightness. From our fits, we obtain that 39% of the light comes from the thick disc. In Salo et al. (2015), this fraction is 33% when using GALFIT3.0 (Peng et al. 2010) for the decomposition (GALFIT3.0, though performing a simultaneous 2D fit over the whole galaxy, oversimplifies the luminosity profiles perpendicular to the mid-planes by assuming that the discs have vertical $\text{sech}^2(z/z_0)$ profiles). The GALFIT3.0 thick disc scale height is

slightly underestimated ($z_T = 3''.4$ for GALFIT3.0 versus $z_T = 4''.4$ in our determination when averaging over the four fits in Fig. 2). GALFIT3.0 finds that the height above which 90% of the light comes from the thick disc is $z = 4''.6$.

4. Observations

The spectroscopic observations were made on the nights 6 – 7 and 7 – 8 of August 2013. We used the integral field unit mode of VIMOS with the High Resolution Blue grism and a spatial resolution of $0''.66 \times 0''.66$ per fibre. The FOV of this mode is

$27'' \times 27''$. The wavelength coverage of this configuration is $3700 - 5350 \text{ \AA}$ and the dispersion is $0.71 \text{ \AA pixel}^{-1}$.

The total in-target exposure was 6.5 hours (2 hours in the first night and 4.5 hours during the second night). The exposure was divided into 13 observing blocks (OBs) with a few arcsecond dithering between them. Each OB exposed ESO 533-4 for 30 minutes. We also took 4 minute exposures of the sky, at a $2'$ distance in the direction perpendicular to the mid-plane. During the first night, a sky exposure was taken for every two galaxy OBs. During the second night two sky exposures were taken for every three galaxy OBs. Both nights were photometric and dark. The seeing was large ($\geq 1''$), but this does not affect our science because in any case we need a large spacial binning to study the thick disc with a sufficiently large signal-to-noise ratio (S/N). Standard calibration exposures (flat fields, bias, calibration lamps) and spectrophotometric standard stars were taken for the two nights.

5. Data reduction

5.1. Basic reduction

First, we used IDL's `LA_COSMIC` routine to clean the cosmic rays. The spectra were reduced and flux calibrated by the VIMOS pipeline. The Reflex environment (Freudling et al. 2013) was used to run the pipeline. VIMOS has four quadrants and the pipeline provides independent reductions for each quadrant. Therefore, the output of the initial reduction was $4 \times 13 = 52$ sets of spectra corresponding to the galaxy.

For each of the quadrants of the sky exposures, we created a single spectrum by averaging the spectra in each spaxel with a 3σ clipping. We calculated the sky emission for each of our galaxy exposures by associating them with the average of the sky spectra from the same quadrant taken within 64 minutes. This time was set so at least one sky exposure could be linked to each galaxy exposure, but in some cases there were up to four. Each of the quadrants has a remarkably uniform sky background. Quadrant number 2 has $\sim 40\%$ less signal than the others.

The information in headers could not be used for spacial alignment because of a few arcsecond imprecisions in the pointing. To circumvent this problem, we tried to align the frames by finding point sources in images made by collapsing the spectra. However, the two point sources in the vicinity of the pointings were close to the edge of the field, and thus did not show up in some of the exposures as a result of the ditherings. Then, we built [OIII] images by integrating in the spectral direction from $\lambda = 5047.5 \text{ \AA}$ to $\lambda = 5054.6 \text{ \AA}$ (this takes the redshift of ESO 533-4 into account). Unresolved star-forming regions stand out in the [OIII] images and were used for manual alignment. Once the galaxy frames were spacially aligned, we summed the spectra for every spaxel using a 3σ clipping. We also summed for each spaxel the sky spectra associated with the galaxy frames that were not clipped away. For every wavelength in each spectrum corresponding to each spaxel, we estimated the S/N by considering the Poisson noise and the readout noise,

$$S/N = \frac{S_{\text{galaxy}}}{\sqrt{S_{\text{galaxy}} + S_{\text{sky}} + \sum_i (RON_i)^2}} \quad (1)$$

where, S_{galaxy} is the signal from the galaxy, S_{sky} is the signal from the sky, and RON_i are the read-out noises of each of the exposures that were summed to obtain the final spectrum of a given spaxel. We neglected the dark current contribution to the

S/N because it is very small (typically $5 e^- \text{ hr}^{-1} \text{ pix}^{-1}$, according to the VIMOS Pipeline User Manual¹).

We masked the two point sources in the field, thought to be foreground stars or ESO 533-4 globular clusters, as well as several spaxels in the edges that were covered by few exposures. The two point sources in the field were used to align the IFU data with the S^4G data. The alignment precision is estimated to be of the order of $1''$.

5.2. Kinematics

5.2.1. Velocity maps

Spacial binning is necessary to achieve a S/N good enough to study thick disc kinematics. The binning was done with the Voronoi binning code by Cappellari & Copin (2003) with the condition of $S/N \sim 25$ for spectral pixels between $\lambda = 4500 \text{ \AA}$ and $\lambda = 5000 \text{ \AA}$.

To find the velocity field of ESO 533-4 we fitted the spacially binned spectra with the MILES stellar population synthesis models (Vazdekis et al. 2010) using the penalized pixel-fitting (pPXF) code by Cappellari & Emsellem (2004)². It is usually required to Gauss-convolve either the library or the observed spectra so their FWHMs match. However, we found that the FWHM in our spectra is $\Delta\lambda \approx 2.2 \text{ \AA}$ on the blue side and $\Delta\lambda \approx 2.8 \text{ \AA}$ on the red side, which is very similar to MILES' FWHM, $\Delta\lambda = (2.51 \pm 0.07) \text{ \AA}$. We therefore decided not to make a convolution. Because of the relatively low S/N of the bins, we only fitted two momenta. Emission lines were masked with a mask $\Delta\nu = 1000 \text{ km s}^{-1}$ in width. We used an eight degree additive Legendre polynomial to correct the continuum shape for dust reddening and possible photometric calibration problems. The velocity map is shown in the right panel in Fig. 3. The height above which 90% of the light comes from the thick disc is $|z| \approx 5''$. Therefore, the uppermost and the lowermost rows of bins should be dominated by the thick disc light.

5.2.2. Rotation curves

We made rotation curves of ESO 533-4 at five different heights, namely $z = 0$, $z = \pm 3''$ ($\sim 0.6 \text{ kpc}$), and $z = \pm 8''$ ($\sim 1.5 \text{ kpc}$; Figure 4). The $z = \pm 8''$ cuts should be well within the region where the light emission comes mostly from the thick disc. The profiles take into account the movement of the Earth away from the galaxy ($\sim 19 \text{ km s}^{-1}$ at the time of the year at which the observations were performed) and assume a heliocentric systemic velocity $v_{\text{sys}} = 2596 \text{ km s}^{-1}$ (Table 2). The points in the rotation curves are calculated by making axial cuts in the data used for Fig. 3. The error bars in the rotation curves are estimated by producing 20 Monte-Carlo simulations (with the estimated noise for each pixel) when obtaining the kinematics from each spectrum.

When extrapolated to $R = 0$, the rotation curves are close to $V = 0$, which confirms that the spectra calibration process is robust. It is also reassuring that our $z = 0$ rotation curve matches very well the $H\alpha$ rotation curve from Mathewson et al. (1992), once this has been offset by $+10 \text{ km s}^{-1}$. The correction seems necessary because taken as it is published, the velocity at $R = 0$ is about -10 km s^{-1} . If the offset is not made, the maximum in the $H\alpha$ rotation curve is found at $v \sim 160 \text{ km s}^{-1}$ on the west-

¹ <ftp://ftp.eso.org/pub/dfs/pipelines/vimos/vimos-pipeline-manual-6.8.pdf>

² Both pPXF and the Voronoi tessellation codes can be found at <http://www-astro.physics.ox.ac.uk/~mxc/software/>

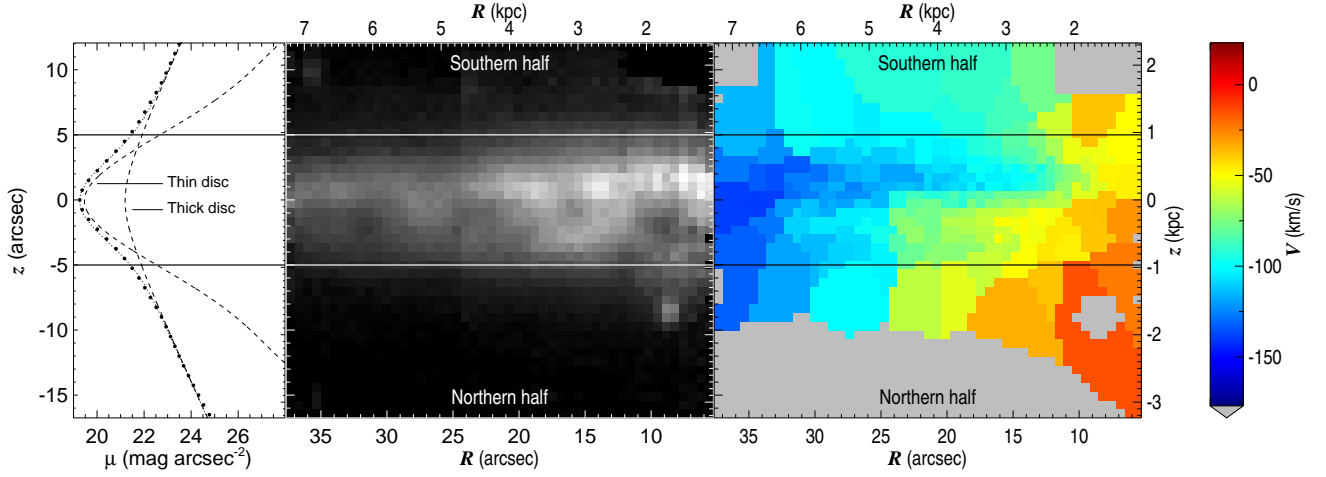


Fig. 3. Left panel: symmetrized, mid-infrared S^4G luminosity profile and thin/thick disc decomposition of the $0.08 r_{25} - 0.69 r_{25}$ ($0.8 - 7.3$ kpc) axial range of ESO 533-4 (the one covered by the IFU). The horizontal solid lines indicate the height, z_s above which 90% of the light comes from the thick disc. Middle panel: image of the observed field made by collapsing the spectra. Right: velocity field of ESO 533-4 after the subtraction of the recession velocity. The horizontal axis indicates the axial distance to the galaxy centre and the vertical axis indicates the distance from the mid-plane.

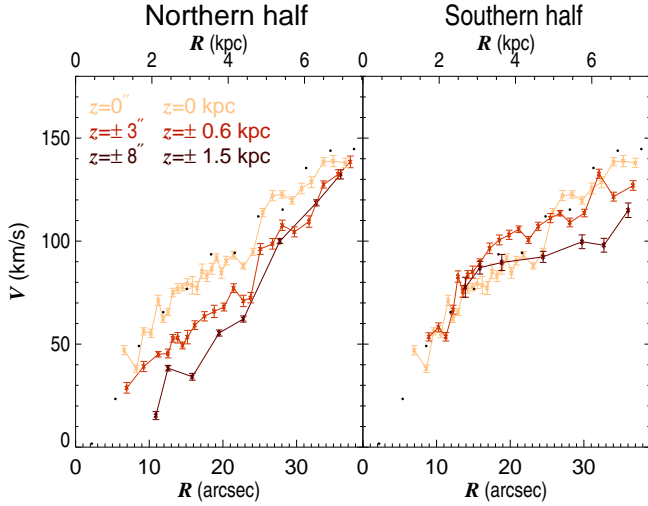


Fig. 4. Rotation curves of ESO 533-4 at different heights as indicated by the colours. The northern half of the disc corresponds to the bottom half of the disc in Fig. 3. The black dots correspond to the Mathewson et al. (1992) $H\alpha$ rotation curve with a $+10 \text{ km s}^{-1}$ offset (see text).

ern side of the galaxy and at $v \sim 140 \text{ km s}^{-1}$ on the eastern side, which would be strange in an undisturbed canonical rotation curve. We suspect an inaccurate calibration or heliocentric correction to be the source of the problems with the $H\alpha$ data as published.

5.3. Stellar populations

To study the stellar populations, we manually created new spacial bins by combining those used in the velocity map. Before summing all the spectra from the low- S/N bins to create the high- S/N binning, we shifted their wavelengths so they all corresponded to a 2500 km s^{-1} recession velocity. We made the bins roughly rectangular, with the long side in the direction of the

plane of the galaxy, so different heights could be studied. To achieve the required S/N for the thick disc, we summed the light from the two sides of the mid-plane. Manual binning is essential because the Voronoi tessellation tries to make “compact” or “round” bins (Cappellari & Copin 2003). This second binning yielded spectra with a $S/N \sim 80$ in the $\lambda = 4500 \text{ \AA}$ to $\lambda = 5000 \text{ \AA}$ spectral range.

To obtain the stellar population map, the spectra were again fitted using pPXF. We used a grid of MILES stellar population templates ranging from 63 Myr to 17.8 Gyr (50 age bins) and from $\log(Z/Z_\odot) = -1.71$ to $\log(Z/Z_\odot) = 0.22$ (six metallicity bins). Thus, the total template number was 300. A regularization factor of $\text{REGUL}=200$ was used to smooth the stellar populations. The continuum was corrected with multiplicative Legendre polynomials (for details on the regularization and the use of Legendre corrective polynomials, see the pPXF documentation). These corrections are essential because of the dust reddening close to the mid-plane and because the blue side of the spectrum has little signal, so it is prone to photometric calibration errors. We tested which polynomial order would work best for our observations. The thick disc fit, where dust reddening is likely to be negligible, is very stable with respect to changes of the order of the polynomial (which indicates little dust affecting the spectra and also a good data calibration that makes correcting polynomials unnecessary). The fitted thin disc stellar populations are very dependent on the order for orders smaller than ~ 10 . For larger orders the fitted stellar populations change little with changes in order, which probably indicates that the continuum shape is properly corrected for differential dust absorption and no further orders are required. The results presented here are fitted with an order 14 polynomial, which is comparable to what others have used with VIMOS data (for example Chilingarian et al. 2009, used 25). The stellar population map is presented in Fig. 5. The fit to the spectra in two of our tiles are shown as an example in Fig. 6. In Fig. 7, mean age and metallicity maps are shown.

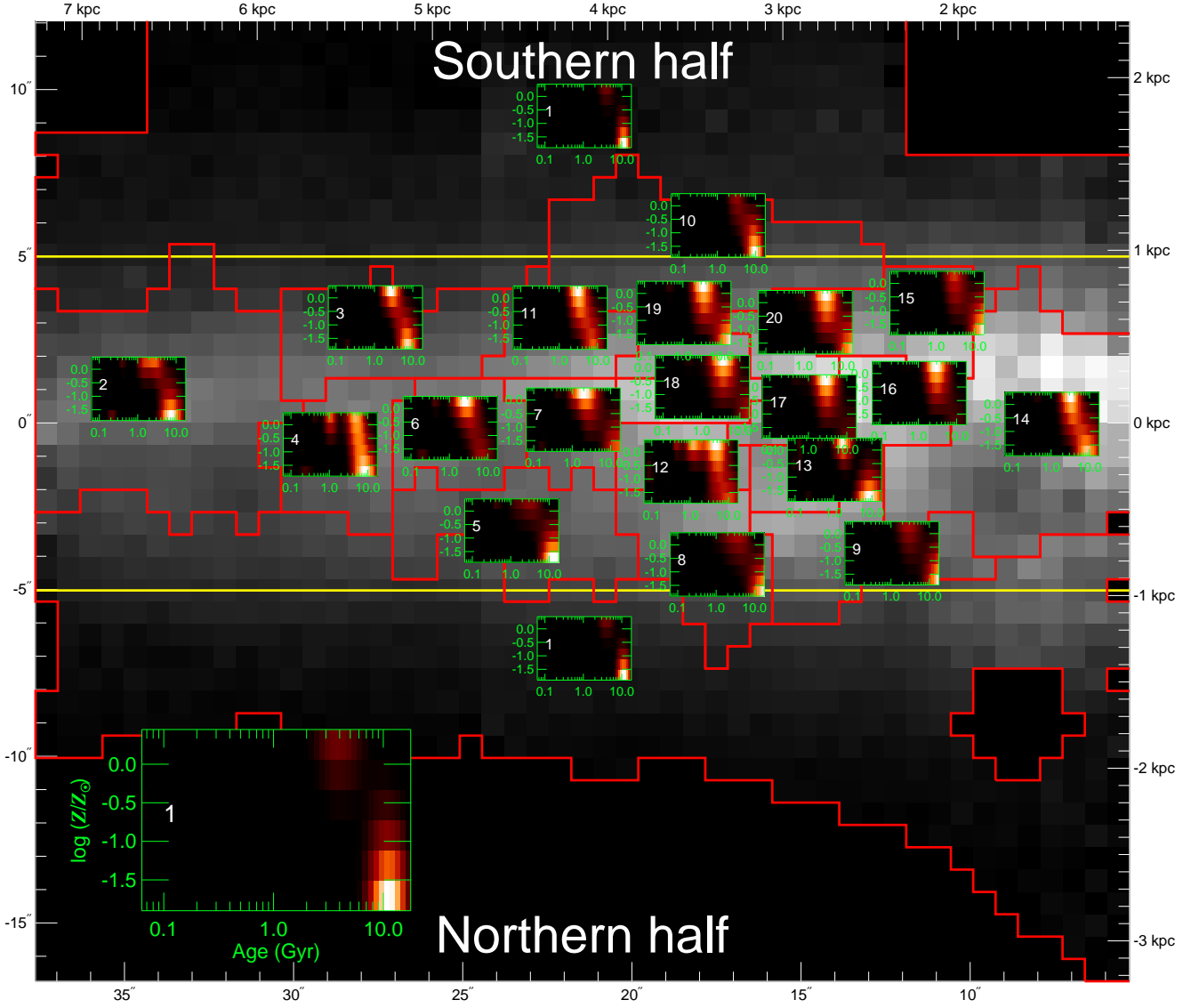


Fig. 5. Stellar populations of ESO 533-4. The background image is the same as in the middle panel of Fig. 3. The red lines indicate the spatial bins used for the analysis. The horizontal solid yellow lines indicate the height above which 90% of the light comes from the thick disc. On top of each bin there is a stellar population plot with the horizontal axis corresponding to the ages in Gyr and the vertical axis corresponding to the metallicities in $\log(Z/Z_{\odot})$. The two thick disc sections (uppermost and lowermost tiles) were actually treated as a single bin. The colours in the plots for each bin indicate the mass fraction of a given stellar population. The bottom left corner of the figure shows an enlarged version of one of the stellar population distributions to improve the readability of the axes.

6. Interpretation of the data

6.1. Kinematics

We find an asymmetry in the velocity map: within the thin disc at a given radius, the southern (upper) half of the galaxy seems to rotate faster than the northern (lower) half (Fig. 3 and the $z = \pm 3''$ or $z = \pm 0.6$ kpc rotation curves in Fig. 4). Possible reasons for the asymmetry are the presence of a dust lane in a not perfectly edge-on disc and features that are not symmetric with respect to the mid-plane (e.g. some phases of a buckling bar such as those seen in Martínez-Valpuesta et al. 2006). The latter possibility, however, is unlikely because there is no sign of a strong bar in ESO 533-4 (boxy/peanut inner isophotes; Combes & Sanders 1981).

The rotation curves for the northern half of the galaxy (below the mid-plane in Fig. 3) decrease monotonically in amplitude as z increases. For the southern half, this is only true for $R \gtrsim 25''$ (a striking feature of the rotation curves is that for the southern half of the galaxy, we find the velocities at $z = 3''$ to be larger than those at $z = 0$ in the $12'' - 25''$ or $2.3 - 4.8$ kpc axial extent). The difference in velocities between the mid-plane and $|z| = 8''$ ($z = \pm 1.5$ kpc) is $10 - 30$ km s $^{-1}$ at the radius where the maximum circular velocity is reached. The apparent rotational lag of the thick disc must at least partly be a consequence of a stronger asymmetric drift caused by the larger velocity dispersion of the thick disc. Part of the lag might be caused by the presence of counter-rotating stars. Finally, part of the apparent lag might be

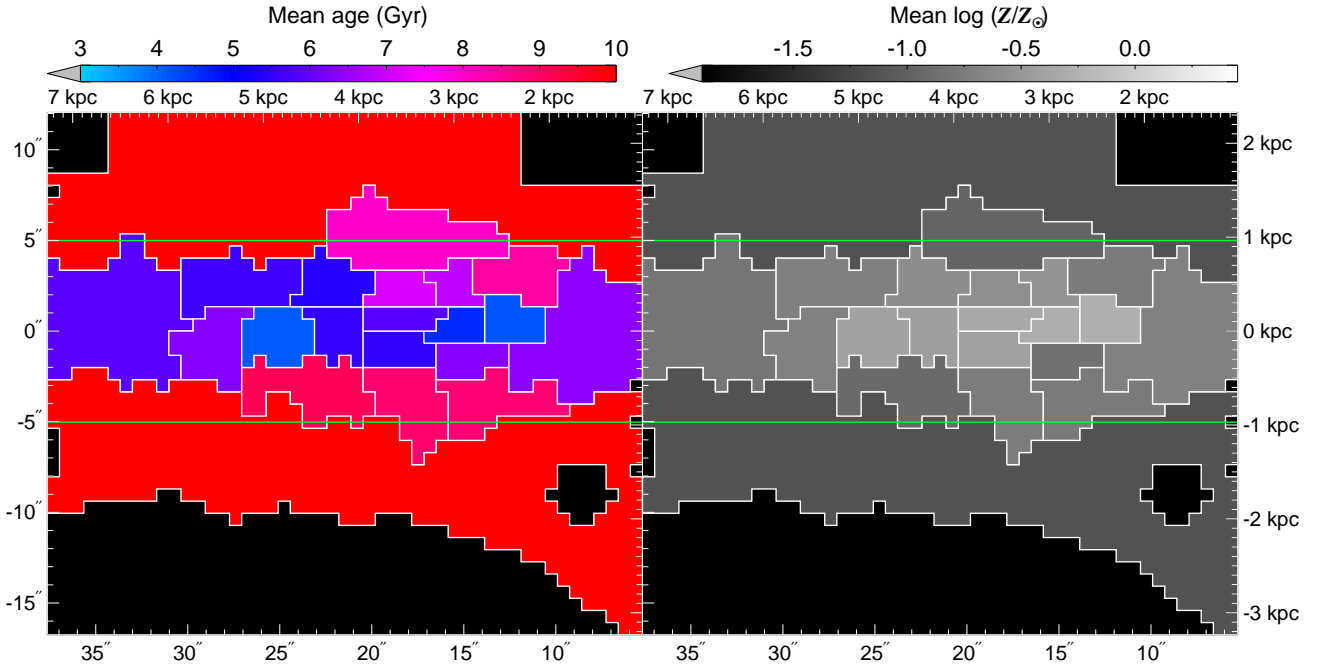


Fig. 7. Mean stellar age (left) and metallicity (right) maps. The white lines indicate the tessellation. The horizontal solid green lines indicate the height above which 90% of the light comes from the thick disc.

because we may be looking at a disc that is not perfectly edge-on.

To check for the causes of the asymmetries in the velocity map and for those of the lag of the thick disc, we ran a set of models using GADGET-2 (Springel 2005). The initial models were created with the GalactICS software (Kuijken & Dubinski 1995). They included a thin disc and a thick disc, which had similar scale lengths. The scale height of the thick disc was ~ 4.9 times larger than that of the thin disc and the mass ratio was 1.1/1.5 in agreement with the values in Table 2 and the fits in Fig. 2. Each of the discs was composed of 1.03×10^6 particles with a Toomre parameter $Q = 1.3$. We also included a small spherical CMC, with a mass 50 times smaller than that of the sum of the two discs, formed of 2×10^4 particles. Finally, we embedded the whole system into a dark matter halo made of 1.08×10^6 particles. The distribution of dark matter particles was set to make a roughly flat rotation curve at large radii. At a radius of two scale lengths the disc contributed to about 40% of the total radial force. The baryonic mass of our model scaled to the observed axial and vertical (Figure 9) profiles and the rotational velocity amplitude is $2.9 \times 10^{10} M_{\odot}$. This is close to the actual mass of ESO 533-4. Models with different dark matter fractions could be created, but then having a good simultaneous vertical and axial match between the models and observations would not have been possible. The model snapshots shown here are for models that have been run for over ten rotations at all the radii covered by the VIMOS observations. This guarantees that the thin and thick discs have settled to equilibrium.

To account for the effect of dust, we assumed it would follow the distribution of thin disc stars except for the fact that we considered a scale height that was three times smaller. We arrived at the ratio of three times smaller because we assumed dust to be mixed with dense gas. In the Milky Way, dense gas has a scale height of ~ 100 pc (Langer et al. 2014) whereas the thin disc scale height is ~ 300 pc (Gilmore & Reid 1983). We assumed the dust would cause a grey absorption, and we studied several

dust densities. The results shown here correspond to an optical depth of $\tau = 8$ to the centre of the galaxy when looking at it from a perfectly edge-on view.

We checked whether ESO 533-4 has some measurable deviation from an edge-on orientation by looking at its colour map (Fig. 8). We found the redder sections of the thin disc to lie slightly below the mid-plane ($\sim 1''$). This implies that the near side of the galaxy is on top, which corresponds to the southern side of the observed galaxy in Fig. 3. We find that a $\sim 1''$ deviation of the dust lane corresponds to a galaxy inclination $i \approx 85^\circ$ in our models. We simulated colour maps by comparing the luminosity profiles of models with and without dust. ESO 533-4's inclination, however, is likely to be closer to 90° given the extremely thin aspect of the disc and the lack of evidence for spiral features (Fig. 1). If the dust distribution were less centrally concentrated than in our models, deviations of only $2-3''$ away from edge-on would be enough to explain the vertical shift of the dust lane. There are clear examples of galaxies where the dust distribution is more extended than that of the stellar disc (e.g. the Sombrero Galaxy or the system studied in Holwerda et al. 2009).

To create synthetic velocity maps, we assigned the MILES spectrum of a 2.5 Gyr star with solar metallicity to thin disc particles. For the thick disc, we used the spectrum of a 10 Gyr star with metallicity $Z = 0.2 Z_{\odot}$. We created synthetic images of the galaxy by projecting them and convolving them with a Gaussian PSF with a FWHM of $1''.2$. We then used the Voronoi tessellation software to create a tessellation matching that obtained for the VIMOS data (i.e. the density of tiles in the thin disc is similar). We then obtained the velocity maps exactly as we did for the VIMOS data.

Figure 10 shows the velocity maps for several models in an area approximately matching that of the VIMOS observations. The top row in the figure corresponds to galaxies with no dust and the bottom row corresponds to galaxies with dust. Models with no dust are symmetric with respect to the mid-

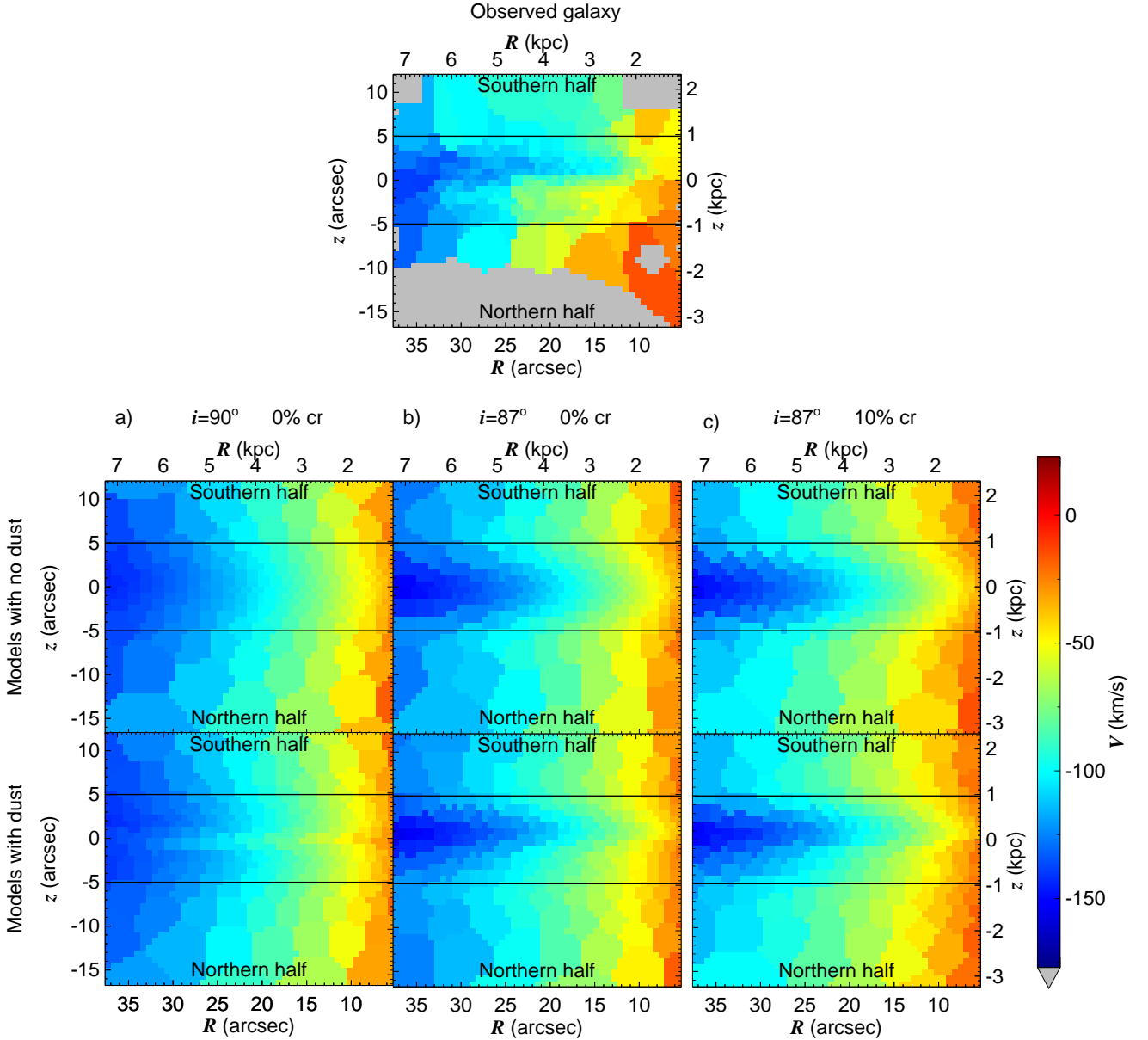


Fig. 10. Top: observed velocity map of ESO 533-4. Middle and bottom rows: set of velocity maps from models designed to mimic the region shown in Fig. 3. The three columns correspond to: a) a perfectly edge-on galaxy with no counter-rotating material; b) a galaxy 3° away from edge-on with no counter-rotating material; and c) a galaxy 3° away from edge-on with 10% of counter-rotating material in the thick disc. The top row corresponds to models with no dust and the bottom row corresponds to models with some amount of dust (see text). The horizontal lines indicate the height above which $\sim 90\%$ of the light comes from the thick disc.

plane. Models with dust, when not seen exactly edge-on, have some degree of asymmetry.

The left column in Fig. 10 corresponds to models with a perfectly edge-on view of the galaxy. The optical depth is the largest close to the mid-plane. Dust attenuates the light from the point which is closer to the galactic centre (that with the largest velocity along the line of sight) more than that of stars closer to the observer. Thus, the dust attenuation causes an apparent slowing of the stars around $z = 0$.

The middle and the right columns in Fig. 10 show that dust is able to create asymmetries when looking at galaxies that are not perfectly edge-on (inclination $i = 87^\circ$ in the example shown here). The larger attenuation on one side of the galaxy causes the asymmetry in the velocity maps: the maximum ve-

locity at a given radius is not found at the mid-plane, but slightly above it. The deviations from symmetry in our models with $i = 87^\circ$ and dust are in qualitative agreement with the observations (Figure 3).

To find the cause of the apparent lag in the thick disc of ESO 533-4 (asymmetric drift, galaxy inclination, and/or presence of counter-rotating stars), we created rotation curves at different heights for the models with the same approach we used for the VIMOS data (Figure 11). We find that at the radius where $v(z = 0) \approx 150 \text{ km s}^{-1}$, the difference in velocity between the mid-plane and $z = \pm 8''$ ($z = \pm 1.5 \text{ kpc}$) is $\sim 20 \text{ km s}^{-1}$ for a model with no counter-rotating material and $\sim 30 \text{ km s}^{-1}$ for a galaxy whose thick disc has 10% of counter-rotating material. These numbers are similar to those observed in ESO 533-4 and

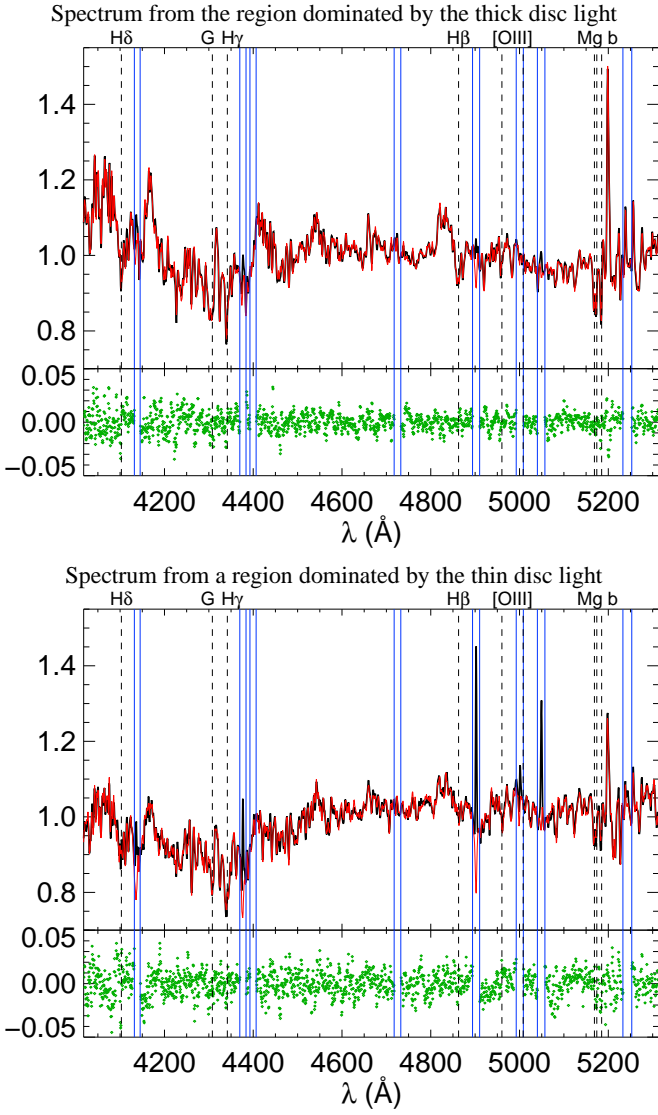


Fig. 6. Two examples of rest-frame spectra obtained from our $S/N \sim 80$ tessellation. The black line corresponds to the actual spectrum, the red line corresponds to the fit, and the blue vertical lines indicate the spectral windows that were masked because of the possible presence of emission lines. Residuals are shown with green symbols below the spectra. The top spectrum belongs to the thick disc dominated region and the bottom spectrum to the rightmost thin disc dominated tile in Fig. 5. The spectra are normalized to their median value. Several spectral lines are indicated with dashed lines.

indicate that the thick disc has little or no counter-rotating material. The effect of the asymmetric drift plus the disc orientation (slightly away from edge-on) are enough to explain the thick disc lag.

In Fig. 11 we see how, in the southern half, the $z = 3''$ ($z = \pm 0.6$ kpc) curve overlaps with that at $z = 0$ for some radial extent. This is because dust absorption is larger at $z = 0$ than at $z = 3''$. By increasing dust absorption it is possible to obtain the $z = 3''$ curve above the $z = 0$ curve for some axial extent just as in the observations. This effect is therefore most likely due to dust.

Our models are not able to reproduce the rotation curves of the northern half of ESO 533-4 for $R < 25''$ ($R < 4.8$ kpc), where

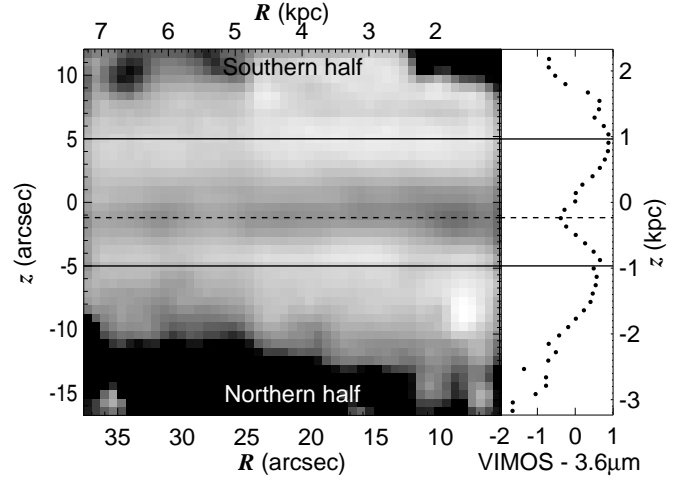


Fig. 8. Left: VIMOS- $3.6 \mu\text{m}$ colour map. The VIMOS image was degraded to the S^4G resolution. Right: median VIMOS- $3.6 \mu\text{m}$ as a function of the height with an arbitrary zero point. The solid horizontal lines indicate the height above which $\sim 90\%$ of the light comes from the thick disc. The dashed horizontal line indicates the reddest height within the thin disc dominated region.

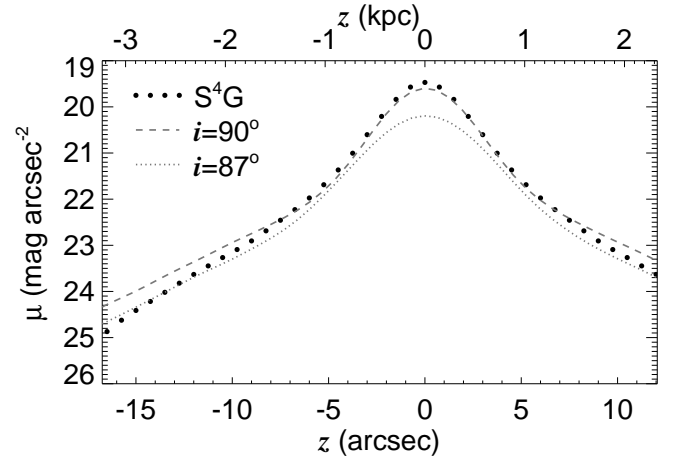


Fig. 9. Luminosity profiles of the observed galaxy (large black dots) and the model galaxies (grey lines) in the $0.08 r_{25} - 0.69 r_{25}$ axial range (dust extinction set to zero). Two models, one with $i = 90^\circ$ (dash), and one with $i = 87^\circ$ (dots), are shown. The zero point of the model profiles is arbitrary.

the thick disc lags by 30 km s^{-1} or more with respect to the mid-plane. The mismatch between the thick disc and the $z = 0$ rotation curves could be due to some fraction of counter-rotating stars in the inner parts of the galaxy. However, if that were the case it would be difficult to explain why the counter-rotating material shows up only on one side of the galaxy.

6.2. Stellar populations

We distinguish two distinct stellar populations in the subplots in Fig. 5. We find:

- an old (~ 10 Gyr) metal-poor population and

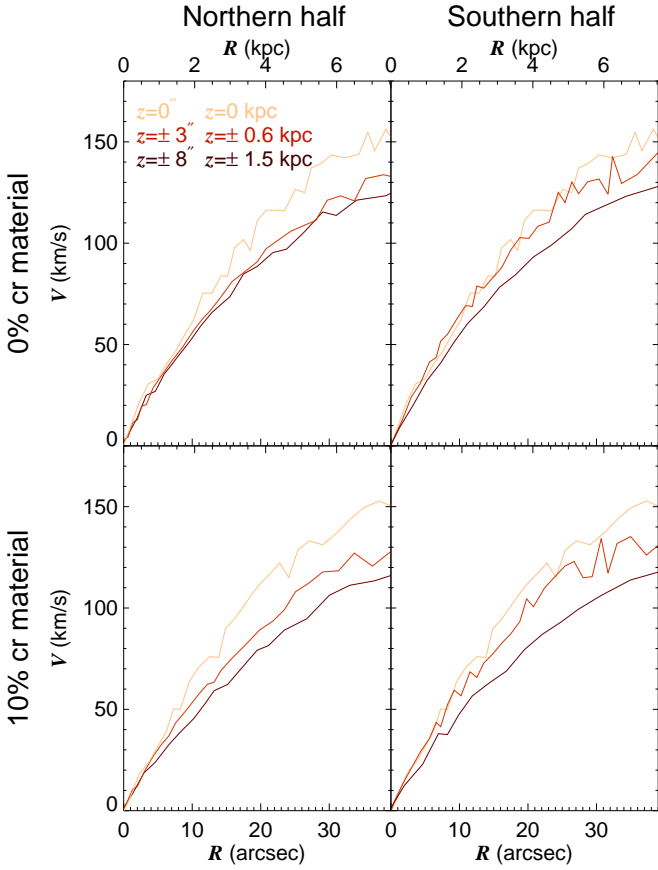


Fig. 11. Rotation curves of models at different heights as indicated by the colours. The northern half of the disc corresponds to the bottom half of the disc in Fig. 10. The top row rotation curves correspond to a model with $i = 87^\circ$, dust and 0% of counter-rotating material, and the bottom row corresponds to similar model with 10% of counter-rotating material in the thick disc.

– a relatively young metal-rich population.

Also, traces of young metal-poor populations, either a fit artefact or associated with the outskirts of the thin disc, are seen in a few of the tiles (this is most evident in the tiles 2, 4, and 6).

To quantify the fraction of mass associated with each of these stellar populations in each tile, we divided the diagrams in two regions, as seen in Fig. 12. The limit between the thin and the thick discs is set at $\log(Z/Z_\odot) = -0.7$ for ages larger than 3 Gyr. All populations younger than 3 Gyr are considered to belong to the thin disc. While a $t = 3$ Gyr stellar population is young compared to what one would expect for a thick disc population, the regularization introduced by pPXF causes stellar populations with peak ages at $t \sim 10$ Gyr to extend down to smaller ages.

The first of the populations in the list is naturally associated with the thick disc, and the second is likely to be related to the thin disc. To further confirm this, we find that the old metal-poor population dominates the mass budget in the bin with the largest height, whereas the younger metal-rich population dominates close to the mid-plane.

In many tiles, the stellar population fits show that the thin and thick disc populations have two distinct maxima in the Age – $\log(Z/Z_\odot)$ plane. In these tiles, the thin and thick disc stars seem to belong to two distinct populations. In other tiles

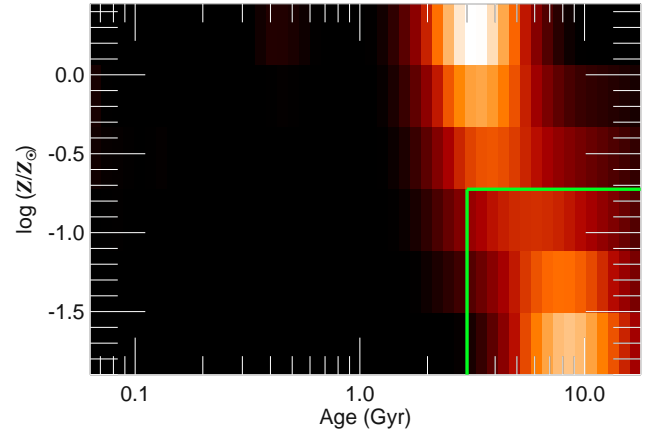


Fig. 12. One of the subplots in Fig. 5 (the rightmost). The green lines indicate the divisions between the thick disc population (bottom right) and the thin disc (rest of the plot).

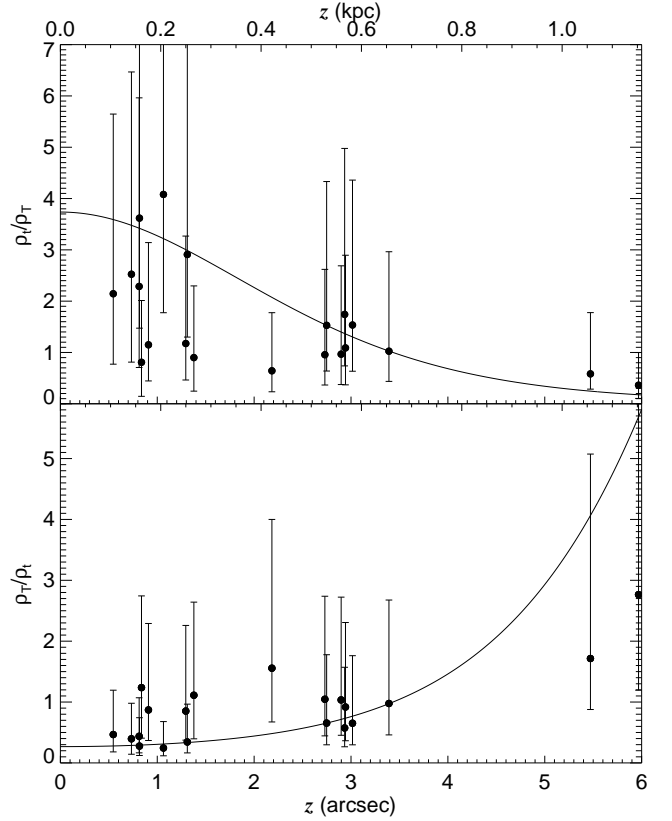


Fig. 13. Ratio between the masses of the thin and thick disc stellar populations (top panel) and its inverse (bottom panel), as a function of the height $|z|$ of the Fig. 5 tile. The lines indicate the same ratios according to the fit to the light profiles (Figure 3).

(particularly 4, 6, 11, and 12 in Fig. 5) the two populations are not so clearly separated. The choice of the regularization parameter introduces a certain arbitrariness in the interpretation of the age-metallicity plane. However, this is a necessary evil, since a certain amount of regularization is needed to smooth the otherwise even more arbitrary solutions of a difficult inverse problem (see pPXF online documentation). While varying the reg-

ularization parameter between $\text{REGUL}=100$ and $\text{REGUL}=250$ does not drastically change the results, higher values can wash out significantly the peaks. The chosen regularization value of $\text{REGUL}=200$ is similar to the value $\text{REGUL}=250$ used in the only source where, to our knowledge, a concrete value of this parameter has been explicitly stated (the example codes from the pPXF website).

If we assume that the stars are divided into a thin and thick disc population (as indicated by many of the $\text{Age} - \log(Z/Z_{\odot})$ plots in Fig. 5), we can test the assumptions made when fitting the luminosity profiles to decompose them into the thin and thick disc components, as in Comerón et al. (2011b,a, 2012, 2014). We calculated for each tile the mass that corresponds to the thin and thick discs according to the fit in the left panel of Fig. 3. To accomplish this, we weighted the spaxels accounting both for the vertical and the axial luminosity profiles (axial luminosity profile from Comerón et al. 2012). Because of the broadness of the peaks that correspond to the stellar populations of the thin and the thick discs (see Fig. 12), the thick disc stellar population might extend to larger metallicities than the ones considered here (limit set at $\log(Z/Z_{\odot}) = -0.7$). Likewise, the thin disc stellar population could extend to smaller metallicities than the ones considered here. To account for this, we considered the possibilities that the thick disc population extended up to $\log(Z/Z_{\odot}) = -0.3$ or only up to $\log(Z/Z_{\odot}) = -1.1$ (for ages larger than 3 Gyr). We also considered the possibilities that the thin disc extended either down to $\log(Z/Z_{\odot}) = -1.1$ or only down to $\log(Z/Z_{\odot}) = -0.3$ for ages larger than 3 Gyr. This is what has been used to calculate the error bars in Fig. 13. The figure shows that the agreement between the results obtained from the stellar population maps and that from our thin/thick disc modelling is good, especially if we take the uncertainties and assumptions made in the modelling process into account.

7. Summary of the results, discussion, and conclusions

In this paper we have made an IFU study of the thin and the thick discs of ESO 533-4 with VIMOS. The main findings are:

- The velocity field of ESO 533-4 is compatible with that of a galaxy inclined a few degrees from edge-on with a significant dust absorption in the equatorial plane. The near side of the galaxy is the southern one.
- The apparent velocity lag of the thick disc can be explained by asymmetric drift and because of the projection effects arising from studying a disc a few degrees ($2 - 3^{\circ}$) away from edge-on. Few or no counter-rotating stars are needed to account for the asymmetric drift of the thick disc.
- The thick disc is made of old (~ 10 Gyr) and metal-poor stars. The thin disc is made of younger metal-rich stars. This is manifested as a distribution with two distinct peaks in the $\text{Age} - \log(Z/Z_{\odot})$ plane for the majority of the regions of ESO 533-4 we studied. This might indicate that the stellar populations of the thin and thick discs are distinct. In several regions (at least 4 out of 20) there is no distinct peaks, but instead a continuum distribution of stellar populations from old metal-poor stars to younger metal-rich stars.
- The relative fractions of mass in the thin and the thick discs at different heights, according to our stellar population analysis, agree with those obtained from our thin/thick disc fits of mid-infrared luminosity profiles.

We first examine the lack of a significant fraction of counter-rotating stars in the thick disc. If the thick disc stars were accreted in a succession of minor mergers, we would expect similar fractions of prograde and retrograde stars, unlike what we observe. If the thick discs were created in a few relatively major mergers (as in e.g. Read et al. 2008) or as a result of the fusion of a few protogalactic mergers, as in Brook et al. (2004), there would be no guarantee that a particular galaxy would have counter-rotating stars. Indeed, in the extreme case where only one such an event occurs, there is a 50% chance of having a prograde merger and a 50% chance of having a retrograde merger. Thus, the lack of counter-rotating material in ESO-533-4 would not rule out a merger origin. If we consider the 1D spectroscopy study by Yoachim & Dalcanton (2008b) and our knowledge of the Milky Way kinematics (Chiba & Beers 2000), we find that none of the five massive galaxies ($v_c \gtrsim 120 \text{ km s}^{-1}$) for which thick disc kinematics are known has a counter-rotating disc. Therefore, if all thick discs in high-mass galaxies share a similar history (which is a reasonable assumption, given that the ratio of the masses of the thin and thick discs are roughly similar for most of the high-mass galaxies; Comerón et al. 2014), a major merger origin is disfavoured by the currently available data. We thus tentatively propose that the thick disc of ESO 533-4 has formed either from dynamical heating or that it was born dynamically hot in a turbulent disc with a large star formation rate.

To distinguish between those two mechanisms, we can use our stellar population data. We see that in most of the tiles in Fig. 5, the thin and the thick disc populations are clearly differentiated in the $\text{Age} - \log(Z/Z_{\odot})$ plane, which would go against a secular heating scenario where a continuous transition between the thin and the thick discs is expected. Instead, it would favour a scenario in which the thick disc became thick at high redshift in a relatively fast process. We however caution against over-interpreting the stellar population results because of the extremely dusty conditions under which the fitting is done and because of their dependence of the smoothing introduced by the regularization of the data. Confirmation of our stellar population results with longer wavelength spectra is thus desirable.

Another and probably more robust way to distinguish between the two mechanisms compatible with our kinematical data is hinted at in Minchev et al. (2015). In their model, age gradients naturally appear in the thick disc-dominated region. These gradients would immediately confirm or infirm the formation scenario where discs are made at high redshift. Unfortunately, because of S/N constrains, we can only make a single bin out of the entire thick disc dominated region, which prevents us from testing for the presence of an age gradient. Even if a larger number of thick disc bins could be made, the effect predicted by Minchev et al. (2015) would be very subtle because our observations extend only out to about 1.5 disc scale lengths (Comerón et al. 2012), whereas a large age difference (of the order of 2 – 4 Gyr) would in theory be observed only over ranges of ~ 3 scale lengths. Larger field of view observations (e.g. with MUSE) are thus needed to settle this issue definitely.

The conclusion is that, if we assume that all thick discs in high-mass galaxies share a common origin, observations favour a dynamical heating or turbulent disc origin for the thick disc in ESO 533-4. A minor merger origin can be discarded, whereas a major merger origin is possible if a variety of scenarios are able to produce a thick disc in high-mass galaxies. The stellar population map of ESO 533-4 is affected by dust absorption and should be interpreted with caution. Recovering the stellar populations from a spectrum is an ill-posed problem which requires

the choice of a regularization parameter to smooth the solution. Having said that, the stellar population fits seem to indicate that this particular galaxy has differentiated thin and thick disc stellar populations, as expected from a short event (either in an early turbulent disc or in a major merger). It thus seems to disfavour a secular evolution origin. A study of the axial gradients of the stellar ages in the thick disc is required to confirm this last assertion.

Acknowledgements. We thank our referee for helping to improve the interpretation of the data. We thank Dr. Michele Cappellari for his help when fitting stellar populations. We thank Dr. Valentin Ivanov for his help during a very complicated observing stint. We thank Dr. Julio Carballo-Bello for pointing out at some useful references. We thank Dr. Frédéric Bournaud for providing details about his simulations. This work is based on observations and archival data made with the Spitzer Space Telescope, which is operated by the Jet Propulsion Laboratory, California Institute of Technology under a contract with NASA. We are grateful to the dedicated staff at the Spitzer Science Center for their help and support in planning and execution of this Exploration Science program. We also gratefully acknowledge support from NASA JPL/Spitzer grant RSA 1374189 provided for the S⁴G project. This research has made use of SAOImage DS9, developed by Smithsonian Astrophysical Observatory. This research has made use of the NASA/IPAC Extragalactic Database (NED), which is operated by the Jet Propulsion Laboratory, California Institute of Technology, under contract with the National Aeronautics and Space Administration. We acknowledge the usage of the HyperLeda database (<http://leda.univ-lyon1.fr>). SC, HS, and EL acknowledge support from the Academy of Finland. JJ thanks the ARC for financial support via DP130100388. The authors acknowledge support for the FP7 Marie Curie Actions of the European Commission, via the Initial Training Network DAGAL under REA grant agreement number 289313.

References

- Abadi, M. G., Navarro, J. F., Steinmetz, M., & Eke, V. R. 2003, *ApJ*, 597, 21
- Alpher, R. A. & Herman, R. C. 1949, *Physical Review*, 75, 1089
- Athanassoula, E. 2013, Bars and secular evolution in disk galaxies: Theoretical input, ed. J. Falcón-Barroso & J. H. Knapen, 305
- Bournaud, F., Elmegreen, B. G., & Martig, M. 2009, *ApJ*, 707, L1
- Bournaud, F., Perret, V., Renaud, F., et al. 2014, *ApJ*, 780, 57
- Brook, C. B., Kawata, D., Gibson, B. K., & Freeman, K. C. 2004, *ApJ*, 612, 894
- Burstein, D. 1979, *ApJ*, 234, 829
- Buta, R. J., Sheth, K., Athanassoula, E., et al. 2015, *ApJS*, 217, 32
- Cappellari, M. & Copin, Y. 2003, *MNRAS*, 342, 345
- Cappellari, M. & Emsellem, E. 2004, *PASP*, 116, 138
- Chiba, M. & Beers, T. C. 2000, *AJ*, 119, 2843
- Chilingarian, I. V., De Rijcke, S., & Buyle, P. 2009, *ApJ*, 697, L111
- Combes, F. & Sanders, R. H. 1981, *A&A*, 96, 164
- Comerón, S., Elmegreen, B. G., Knapen, J. H., et al. 2011a, *ApJ*, 741, 28
- Comerón, S., Elmegreen, B. G., Knapen, J. H., et al. 2011b, *ApJ*, 738, L17
- Comerón, S., Elmegreen, B. G., Salo, H., et al. 2012, *ApJ*, 759, 98
- Comerón, S., Elmegreen, B. G., Salo, H., et al. 2014, *A&A*, 571, A58
- Comerón, S., Knapen, J. H., Sheth, K., et al. 2011c, *ApJ*, 729, 18
- Curtis, H. D. 1917, *PASP*, 29, 206
- de Vaucouleurs, G., de Vaucouleurs, A., Corwin, Jr., H. G., et al. 1991, Third Reference Catalogue of Bright Galaxies. Volume I: Explanations and references. Volume II: Data for galaxies between 0^h and 12^h. Volume III: Data for galaxies between 12^h and 24^h.
- Elmegreen, B. G. & Elmegreen, D. M. 2006, *ApJ*, 650, 644
- Freudling, W., Romaniello, M., Bramich, D. M., et al. 2013, *A&A*, 559, A96
- Gamow, G. 1946, *Physical Review*, 70, 572
- Gilmore, G. & Reid, N. 1983, *MNRAS*, 202, 1025
- Holwerda, B. W., Keel, W. C., Williams, B., Dalcanton, J. J., & de Jong, R. S. 2009, *AJ*, 137, 3000
- Hubble, E. P. 1925, *ApJ*, 62, 409
- Johnston, K. V., Bullock, J. S., Sharma, S., et al. 2008, *ApJ*, 689, 936
- Kormendy, J. & Kennicutt, Jr., R. C. 2004, *ARA&A*, 42, 603
- Kuijken, K. & Dubinski, J. 1995, *MNRAS*, 277, 1341
- Langer, W. D., Pineda, J. L., & Velusamy, T. 2014, *A&A*, 564, A101
- Le Fèvre, O., Saisse, M., Mancini, D., et al. 2003, in Society of Photo-Optical Instrumentation Engineers (SPIE) Conference Series, Vol. 4841, Instrument Design and Performance for Optical/Infrared Ground-based Telescopes, ed. M. Iye & A. F. M. Moorwood, 1670–1681
- Lemaître, G. 1931, *Nature*, 127, 706
- Loebman, S. R., Roškar, R., Debattista, V. P., et al. 2011, *ApJ*, 737, 8
- Makarov, D., Prugniel, P., Terekhova, N., Courtois, H., & Vauglin, I. 2014, *A&A*, 570, A13
- Martinez-Valpuesta, I., Shlosman, I., & Heller, C. 2006, *ApJ*, 637, 214
- Mathewson, D. S., Ford, V. L., & Buchhorn, M. 1992, *ApJS*, 81, 413
- Minchev, I., Famaey, B., Quillen, A. C., et al. 2012, *A&A*, 548, A127
- Minchev, I., Martig, M., Streich, D., et al. 2015, *ApJ*, 804, L9
- Muñoz-Mateos, J. C., Sheth, K., Regan, M., et al. 2015, *ApJS*, 219, 3
- Narayan, C. A. & Jog, C. J. 2002, *A&A*, 394, 89
- Nykytyuk, T. V. & Mishenina, T. V. 2006, *A&A*, 456, 969
- Öpik, E. 1922, *ApJ*, 55, 406
- Peng, C. Y., Ho, L. C., Impey, C. D., & Rix, H.-W. 2010, *AJ*, 139, 2097
- Penzias, A. A. & Wilson, R. W. 1965, *ApJ*, 142, 419
- Planck Collaboration. 2015, *A&A*, submitted, arXiv:1502.01589
- Qu, Y., Di Matteo, P., Lehnert, M. D., & van Driel, W. 2011, *A&A*, 530, A10
- Quinn, P. J., Hernquist, L., & Fullagar, D. P. 1993, *ApJ*, 403, 74
- Read, J. I., Lake, G., Agertz, O., & Debattista, V. P. 2008, *MNRAS*, 389, 1041
- Roškar, R., Debattista, V. P., & Loebman, S. R. 2013, *MNRAS*, 433, 976
- Salo, H., Laurikainen, E., Laine, J., et al. 2015, *ApJS*, 219, 4
- Sandin, C. 2015, *A&A*, 577, A106
- Schönrich, R. & Binney, J. 2009a, *MNRAS*, 396, 203
- Schönrich, R. & Binney, J. 2009b, *MNRAS*, 399, 1145
- Sheth, K., Regan, M., Hinz, J. L., et al. 2010, *PASP*, 122, 1397
- Skrutskie, M. F., Cutri, R. M., Stiening, R., et al. 2006, *AJ*, 131, 1163
- Springel, V. 2005, *MNRAS*, 364, 1105
- Streich, D., de Jong, R. S., Bailin, J., et al. 2015, *ArXiv e-prints*
- Toomre, A. 1977, in *Evolution of Galaxies and Stellar Populations*, ed. B. M. Tinsley & R. B. G. Larson, D. Campbell, 401
- Tsikoudi, V. 1979, *ApJ*, 234, 842
- Vazdekis, A., Sánchez-Blázquez, P., Falcón-Barroso, J., et al. 2010, *MNRAS*, 404, 1639
- Vera-Ciro, C., D’Onghia, E., Navarro, J., & Abadi, M. 2014, *ApJ*, 794, 173
- Villumsen, J. V. 1985, *ApJ*, 290, 75
- Yoachim, P. & Dalcanton, J. J. 2006, *AJ*, 131, 226
- Yoachim, P. & Dalcanton, J. J. 2008a, *ApJ*, 683, 707
- Yoachim, P. & Dalcanton, J. J. 2008b, *ApJ*, 682, 1004
- Zaritsky, D., Courtois, H., Muñoz-Mateos, J.-C., et al. 2014, *AJ*, 147, 134